Acta Crystallographica Section D
Biological Crystallography
ISSN 1399-0047

The structure of allophycocyanin B from *Synechocystis* PCC 6803 reveals the structural basis for the extreme redshift of the terminal emitter in phycobilisomes

Pan-Pan Peng,[a] Liang-Liang Dong,[a] Ya-Fang Sun,[a] Xiao-Li Zeng,[a] Wen-Long Ding,[a] Hugo Scheer,[b] Xiaojing Yang[c]* and Kai-Hong Zhao[a]*

[a]State Key Laboratory of Agricultural Microbiology, Huazhong Agricultural University, Wuhan 430070, People's Republic of China, [b]Department Biologie I, Universität München, Menzinger Strasse 67, D-80638 München, Germany, and [c]Department of Biochemistry and Molecular Biology, The University of Chicago, Chicago, IL 60637, USA

Correspondence e-mail: xiaojing@uic.edu, khzhao@163.com

Received 31 March 2014
Accepted 6 July 2014

PDB reference:
allophycocyanin B, 4po5

Allophycocyanin B (AP-B) is one of the two terminal emitters in phycobilisomes, the unique light-harvesting complexes of cyanobacteria and red algae. Its low excitation-energy level and the correspondingly redshifted absorption and fluorescence emission play an important role in funnelling excitation energy from the hundreds of chromophores of the extramembraneous phycobilisome to the reaction centres within the photosynthetic membrane. In the absence of crystal structures of these low-abundance terminal emitters, the molecular basis for the extreme redshift and directional energy transfer is largely unknown. Here, the crystal structure of trimeric AP-B [$(ApcD/ApcB)_3$] from *Synechocystis* sp. PCC 6803 at 1.75 Å resolution is reported. In the crystal lattice, eight trimers of AP-B form a porous, spherical, 48-subunit assembly of 193 Å in diameter with an internal cavity of 1.1×10^6 Å^3. While the overall structure of trimeric AP-B is similar to those reported for many other phycobiliprotein trimers, the chromophore pocket of the α-subunit, ApcD, has more bulky residues that tightly pack the phycocyanobilin (PCB). Ring D of the chromophores is further stabilized by close interactions with ApcB from the adjacent monomer. The combined contributions from both subunits render the conjugated rings B, C and D of the PCB in ApcD almost perfectly coplanar. Together with mutagenesis data, it is proposed that the enhanced planarity effectively extends the conjugation system of PCB and leads to the redshifted absorption (λ_{max} = 669 nm) and fluorescence emission (679 nm) of the ApcD chromophore in AP-B, thereby enabling highly efficient energy transfer from the phycobilisome core to the reaction centres.

1. Introduction

Cyanobacteria and red algae thrive in a large variety of habitats. Using a unique antenna complex, the phycobilisome (PBS), they harvest a significant portion of the solar energy which is globally used by natural photosynthesis. PBSs are supramolecular complexes of sizes up to 8 MDa comprising brightly coloured phycobiliproteins carrying a variety of linear tetrapyrrole chromophores and organizing linker proteins. Trimers [heterohexamers, $(\alpha\beta)_3$[1]] of phycoerythrin, phycoerythrocyanin, phycocyanin (CPC) and allophycocyanin (APC) collect light efficiently in the spectral range 480–650 nm where chlorophylls absorb only poorly (Glazer, 1984; Sidler, 1994; MacColl, 1998; Gantt *et al.*, 2003). This energy is transferred from the PBS to the chlorophyll *a*-containing

[1] In the following, the heterodimeric $\alpha\beta$ protomer will be called a monomer and larger aggregates will be named according to the number of such monomers that they contain.

reaction centres (RCs) of photosystems I and II *via* two terminal emitters (Glazer, 1984; Sidler, 1994): allophycocyanin B (AP-B) and the core–membrane linker (L_{CM}) (Glazer & Bryant, 1975; Gingrich *et al.*, 1983; Lundell & Glazer, 1983*a*; Ducret *et al.*, 1998; Dong *et al.*, 2009; Liu *et al.*, 2013).

Together with L_{CM} and the small core linker (L_C), APC and AP-B form the PBS core (Gingrich *et al.*, 1983; Ducret *et al.*, 1998). The low energy levels of AP-B and L_{CM} ($\lambda_{max,absorption} \simeq 670$ nm; $\lambda_{max,emission} \simeq 675$ nm) allow optimal energy transfer from the large number of higher-energy chromophores of the peripheral phycobiliproteins to the chlorophylls of the membrane-bound RC. Both AP-B and APC contain the same phycocyanobilin (PCB) chromophores as the much more abundant CPCs, but their spectra are considerably redshifted. In APC, a ~30 nm redshift is induced upon trimer formation by a mechanism that is still under debate (MacColl, 2004; McGregor *et al.*, 2008; Csatorday *et al.*, 1984): APC monomers ($\alpha\beta$) absorb at 615 nm, while trimers absorb at 652 nm and fluoresce at 660 nm. Monomers of AP-B absorb at 621–648 nm (Lundell & Glazer, 1981); the redshift upon aggregation results in trimers that absorb at ~670 nm and fluoresce at ~675 nm (Lundell & Glazer, 1983*a*). AP-B differs from APC in that the α-subunit ApcA is replaced by the homologous ApcD, which carries the redshifted PCB (Lundell & Glazer, 1981; Zhao, Su *et al.*, 2007). While crystal structures have been solved for most of the abundant phycobiliproteins, the structural basis for the redshift of the terminal emitters AP-B and L_{CM} is still lacking (Schirmer *et al.*, 1985, 1986; Ficner *et al.*, 1992; Brejc *et al.*, 1995; Reuter *et al.*, 1999; Stec *et al.*, 1999; Wang *et al.*, 2001; Adir & Lerner, 2003; David *et al.*, 2011; Liu *et al.*, 1999; Marx & Adir, 2013; Adir *et al.*, 2002).

In PBS, both AP-B and L_{CM} are in very low abundance. ApcD expressed in *Escherichia coli* has been assembled with PCB *in vitro* (Zhao, Su *et al.*, 2007) but could not be crystallized, likely owing to incomplete chromophorylation. We have now inserted the coding sequence for a C-terminal His tag into ApcD from the genome of *Synechocystis* sp. PCC 6803 (*Synechocystis*), which allowed the purification of AP-B *via* affinity chromatography and subsequent crystallization. The crystal structure determined at 1.75 Å resolution revealed a striking spherical packing of an ApcD–ApcB trimer in the crystal lattice. Comparisons with other phycobiliproteins provide insight into the structural origin of the unusually redshifted spectra of the PCB chromophore of ApcD in AP-B.

2. Experimental procedures

2.1. Bacterial strains and growth media

Axenic cells of *Synechocystis* sp. strain PCC 6803 (*Synechocystis*), a glucose-tolerant strain provided by the Institute of Hydrobiology, Chinese Academy of Sciences, Wuhan, People's Republic of China, were grown in BG11 medium supplemented with kanamycin (30 mg ml^{-1}), if necessary, in Erlenmeyer flasks at 30°C under continuous white light (fluorescent lamp, photon flux density 20 mmol m^{-2} s^{-1}). The flasks were bubbled with a continuous stream of air containing 0.04%(*v*/*v*) CO_2. Growth was monitored by measuring the absorbance at 730 nm (OD_{730}) using an absorption spectrophotometer (Beckman–Coulter DU 800). The cells were harvested at mid-exponential stage by centrifugation (12 000*g*, 5 min, 4°C), washed twice with water and stored at −20°C until use. Cells were grown on plates using the same light intensities on BG11 medium solidified with 1.5% agar (Sokolenko *et al.*, 2002).

2.2. Generation of *Synechocystis* mutants

All genetic manipulations were carried out according to standard protocols (Sambrook *et al.*, 1989). The *apcD* (*sll0928*) region (0.5 kb) was amplified *via* PCR with primers P1 and P2 that contain the His-tag sequence (Supplementary Table S1[2]). The amplified fragment was then cloned into pBluescript KS(+) between the *Eco*RI and *Xho*I restriction sites to yield pBlue-*apcD-histag* (Supplementary Fig. S1). The DNA fragment encoding the *apcD* downstream sequence (0.8 kb) was PCR-amplified using primers P3 and P4 containing *Eco*RI and *Xba*I restriction sites (Supplementary Table S1). Insertion of the DNA fragment into pBlue-*apcD-histag* resulted in pBlue-*apcD-histag*-downstream. This was digested with *Eco*RI and the resulting fragment was blunted with Klenow fragment. The *aph*II gene (aminoglycoside 3′-phosphotransferase II) conferring kanamycin resistance (Km^R) was cut from pCOLADuet with *Eco*RV. After purification, the two blunt fragments were ligated to yield pBlue-*apcD-histag*-Km^R-downstream (Supplementary Fig. S1). The correct sequence of the pBlue-*apcD-histag*-Km^R-downstream construct was verified before transforming *Synechocystis* cells (Golden *et al.*, 1987). Transformants were streaked on BG11 plates containing kanamycin (30 mg ml^{-1}). Segregation of a mutant was achieved by re-streaking 2–3 times on these kanamycin plates. Complete segregation of the mutant was checked by PCR (Supplementary Fig. S1).

2.3. Generation of ApcD mutants in *E. coli*

Chromophorylation of ApcD and its mutants with PCB in *E. coli* was carried out as reported previously (Zhao, Su *et al.*, 2007; Wang *et al.*, 2010). *apcD* from *Synechocystis* was cloned into pET-30 to yield pET-apcD and the mutations were then introduced as summarized in Supplementary Table S1. For assembly in *E. coli*, three plasmids (pCDF-cpcS for S-type lyase, pACYC-ho1-pcyA for PCB, and pET derivatives for apoproteins; Supplementary Table S2) were co-transformed into *E. coli* BL21(DE3). For expression, cells were grown at 20°C in LB medium containing kanamycin (20 µg ml^{-1}), chloromycetin (17 µg ml^{-1}) and streptomycin (25 µg ml^{-1}). 12 h after induction with IPTG (1 m*M*), the cells were collected by centrifugation, washed twice with distilled water and stored at −20°C until use.

[2] Supporting information has been deposited in the IUCr electronic archive (Reference: TZ5058).

2.4. Purification of AP-B and chromophorylated ApcD

ApcD and AP-B carrying a His tag were purified from *Synechocystis* as follows. The cell pellet was resuspended in ice-cold 20 m*M* potassium phosphate buffer (KPB) pH 7.2 containing 0.3 *M* NaCl and disrupted using a French press. The suspension was centrifuged at 12 000*g* for 30 min at 4°C and the supernatant was loaded onto an Ni^{2+}-affinity column (Chelating Sepharose, Amersham Biosciences) equilibrated with 20 m*M* KPB pH 7.2 containing 0.3 *M* NaCl. After exhaustive washing to remove the unbound fractions, the bound proteins were eluted with 20 m*M* KPB pH 7.2 containing an additional 0.25 *M* imidazole. The collected fractions were dialyzed against 1 *M* KPB pH 7.2. The affinity-enriched protein was further purified *via* FPLC (Amersham Biosciences) using either a Superose 6 column equilibrated with 1 *M* KPB pH 7.2 or a Superdex 200 column equilibrated with 20 m*M* KPB pH 7.2 containing 0.1 *M* NaCl.

2.5. Protein assay and aggregation state

Protein concentrations were determined by the Bradford assay (Bradford, 1976) calibrated with bovine serum albumin. SDS–PAGE was performed using the buffer system of Laemmli (1970). Proteins were stained with Coomassie Brilliant Blue and those containing chromophores were further identified by Zn^{2+}-induced fluorescence (Berkelman & Lagarias, 1986).

To determine the oligomerization state of the isolated AP-B, it was first purified by Zn^{2+}-affinity chromatography and Superose 6 gel-filtration chromatography. 1 ml of the eluate (0.5 m*M*) was loaded onto a Superdex 200 column (60 × 1.6 cm) and eluted (1.0 ml min^{-1}) with 20 m*M* KPB pH 7.2 containing 0.1 *M* NaCl. The apparent molecular mass was determined by comparison with a marker set (29–700 kDa; Sigma–Aldrich). For dissociation experiments, the same procedure was used but the elution buffer was supplemented with urea.

2.6. Two-dimensional electrophoresis of AP-B and the identification of AP-B subunits

The purified protein sample was loaded onto an Ettan IPGphor3 (GE Healthcare) two-dimensional electrophoresis apparatus. The first dimension was isoelectric focusing (IEF). Immobilized polyacrylamide gel (IPG) strips (18 cm, pH 4.0–7.0) were developed for 26 h at 30–10 000 V in 2% CHAPS buffer containing 40 m*M* DTT and 6 *M* urea plus 2 *M* thiourea. The IEF points for each subunit of AP-B were determined by scaling. The second dimension was SDS–PAGE using an Ettan DALTsix multiple-gel electrophoresis unit (GE Healthcare).

The protein bands were extracted and were subsequently identified by Shanghai Applied Protein Technology Co. Ltd by mass spectrometry using a 4800 Plus MALDI TOF/TOF Analyzer (AB SCIEX). Proteins were identified with *Mascot* using the National Center for Biotechnology Information database (http://www.matrixscience.com/search_form_select.html).

2.7. Spectral analyses

UV–Vis absorption and CD spectra were recorded using a model DU 800 spectrophotometer (Beckman–Coulter) and a MOS-500 (Bio-Logic) spectropolarimeter equipped with a stopped-flow unit, respectively. Fluorescence spectra were measured using an LS 55 spectrofluorimeter (Perkin–Elmer). The covalently bound PCB in phycobiliproteins was quantified after denaturation with acidic urea (8 *M*, pH 1.5) by the absorption of PCB at 662 nm (ε = 35 500 M^{-1} cm^{-1}; Glazer & Fang, 1973). Fluorescence quantum yields, Φ_F, were determined in 20 m*M* KPB pH 7.2 using the known Φ_F = 0.27 for CPC from *Nostoc* sp. PCC 7120 (Cai *et al.*, 2001) as a standard.

2.8. Electron microscopy

The AP-B sample (10 mg ml^{-1} in 20 m*M* KPB pH 7.2 containing 0.3 *M* NaCl) deposited on a copper grid was stained with 2% uranium acetate for 3–5 min. After air drying, the sample on the grid was inspected using a 100 kV transmission electron microscope (Hitachi 3H-7000FA).

2.9. Crystallization and data collection

AP-B (15 mg ml^{-1}) was crystallized by the hanging-drop vapour-diffusion method at 293 K using mother liquor consisting of 0.5 *M* ammonium sulfate, 0.1 *M* sodium citrate tribasic dihydrate pH 5.6, 1.0 *M* lithium sulfate monohydrate. AP-B crystals were harvested and flash-cooled using liquid nitrogen with no additional cryoprotectant. All X-ray diffraction data were collected on the LS-CAT beam stations at the Advanced Photon Source, Argonne National Laboratory, USA. All diffraction data were processed using *HKL-2000* (Otwinowski & Minor, 1997). The crystal structure was determined at 1.75 Å resolution by molecular replacement with *Phaser* using the ApcA–ApcB monomer (PDB entry 1b33; Reuter *et al.*, 1999) as a search model and was refined to a final *R* factor and free *R* factor of 0.169 and 0.193, respectively, using *PHENIX* (Adams *et al.*, 2010). Analysis of buried surface areas was carried out using the *PISA* server (http://www.ebi.ac.uk/pdbe/prot_int/pistart.html; Krissinel & Henrick, 2007). Statistics of data collection and structural refinement are summarized in Table 1. The coordinates and structure-factor amplitudes of the AP-B structure have been deposited in the Protein Data Bank as entry 4po5.

3. Results

3.1. Purification, composition and spectra of AP-B from *Synechocystis*

After linking an 18-base segment coding for a C-terminal His tag to *apcD*, the AP-B complex was isolated from transformed *Synechocystis* by Ni^{2+}-affinity chromatography using KPB buffer of low ionic strength (20 m*M*) containing 300 m*M* NaCl. When cell disintegration and Ni^{2+}-affinity chromatography were carried out using KPB buffer of high ionic strength (1 *M*), intact PBS could be isolated (not shown), indicating that His-tagged ApcD was assembled in the PBS.

Table 1
Data-collection and refinement statistics for AP-B from *Synechocystis*.

Data processing	*HKL*-2000
Beamline	LS-CAT 21-ID-G, APS
Space group	*I*422
Unit-cell parameters (Å)	$a = b = 184.3$, $c = 260.9$
Wavelength (Å)	0.97857
Resolution (Å)	1.75
R_{merge} (%)	0.052
$\langle I/\sigma(I)\rangle$	23.8
Completeness (%)	98.6
Multiplicity	6.6
Structure refinement	
R factor/R_{free} (%)	0.169/0.193
Resolution (Å)	1.75
Average B value (Å^2)	21.5
R.m.s. deviations	
Bonds (Å)	0.009
Angles (°)	1.507
Ramachandran plot (%)	
Favoured	97.8
Allowed	1.85
Disallowed	0.35 (Thr74*B*)
Asymmetric unit contents	3 ApcD, 3 ApcB, 6 PCB, 1193 waters, 21 sulfates
PDB code	4po5

Dissociation of the PBS in KPB of low ionic strength (20 m*M*) resulted in AP-B after Ni^{2+}-affinity chromatography but with lower yields. Therefore, all subsequent experiments were performed using 20 m*M* KPB throughout.

Two-dimensional electrophoresis (Fig. 1) of AP-B showed two or three spots. The former preparations contained two proteins in the 18 kDa range that fluoresce under Zn^{2+} induction (Berkelman & Lagarias, 1986), indicating that the complex contains two bilin-binding subunits. According to the isoelectric focusing dimension, their isoelectric points are 5.12 and 6.38 (Fig. 1), which agree well with the calculated pIs of ApcB (5.43) and ApcD (6.37), respectively. MALDI-TOF mass spectrometry confirmed these assignments (Supplementary Fig. S2). The spot densities of 1:1.02 on the two-dimensional gels agree with a 1:1 ApcD:ApcB composition (or multiples thereof) in the AP-B complex. The calculated molecular mass of the monomer, 36 kDa, is about one third of that observed in gel filtration (Supplementary Fig. S3), indicating a trimeric aggregate. There was no evidence for the existence of a core linker, L_C, with a molecular weight of ∼10 kDa in the complex (Supplementary Fig. S3). Early isolations of AP-B were devoid of L_C (Lundell & Glazer, 1981), while this linker can be retained under milder conditions (Gingrich *et al.*, 1983; Reuter *et al.*, 1990; Redecker *et al.*, 1993).

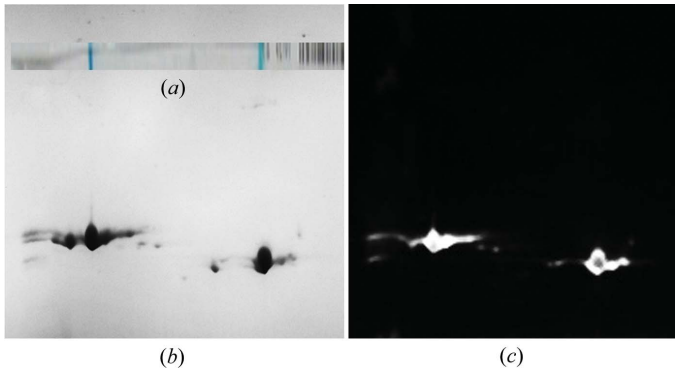

Figure 1
Two-dimensional electrophoresis of AP-B. The sample was purified by Ni^{2+}-affinity chromatography and subsequent gel filtration over Superose 6. (*a*) Isoelectric focusing (IEF) of the first dimension, with spots corresponding to pI values of 5.13 (left) and 6.41 (right). The calculated pIs are 5.43 for ApcB and 6.37 for ApcD, respectively; these assignments were confirmed by MALDI-TOF mass spectrometry (Supplementary Fig. S2). (*b*) Two-dimensional gel stained with Coomassie Brilliant Blue. (*c*) Zinc-induced fluorescence of the two-dimensional gel shown in (*b*). Densitometry resulted in a subunit composition ApcD:ApcB $\simeq$ 1:1.02. Within the error limits, this suggests a composition ApcD–ApcB.

Some AP-B isolates contained a third protein that was identified by two-dimensional electrophoresis and mass spectrometry (not shown) as chromophorylated ApcA. It does not seem to matter whether ApcA is present or not: all of the preparations resulted in crystals that contained only ApcB and ApcD (see below). The following characterization was performed with preparations containing only ApcB and ApcD.

The purified AP-B trimer has two overlapping absorption bands with peaks at 618 and 669 nm and showed a single, unstructured emission peak at 679 nm (Fig. 2). AP-B was quite stable against dilution. When titrated with urea, dissociation to monomers was complete at 2 *M* as judged by gel filtration, which was accompanied by the disappearance of the redshifted absorption and fluorescence (Supplementary Fig. S4). This behaviour is similar to that of APC (MacColl, 2004), but in AP-B the absorptions of both the monomer and the

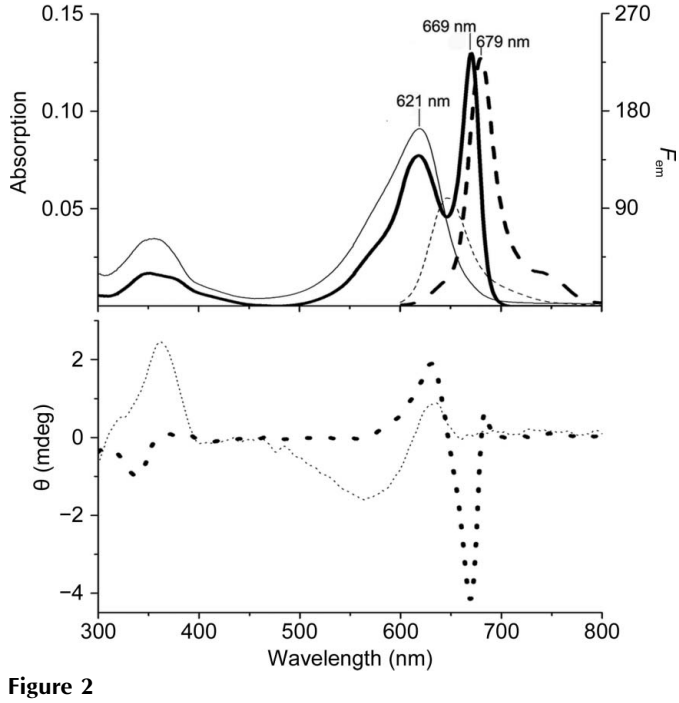

Figure 2
Absorption (unbroken lines), fluorescence (dashed lines) and CD (dotted lines) spectra of AP-B. Thick lines are the spectra of trimers, $(ApcD–ApcB)_3$, recorded in 20 m*M* KPB pH 7.2 containing 0.1 *M* NaCl; the thin lines are the spectra of monomers obtained from the same samples after the addition of 2 *M* urea. More detailed spectral characteristics are shown in Supplementary Fig. S4. AP-B was purified by Ni^{2+}-affinity chromatography followed by gel filtration on Superose 6 (see §2 for details).

trimer are redshifted by ∼20 nm. A similar redshift is seen in the CD spectrum of monomeric AP-B compared with APC, but the CD of the trimers differs substantially: APC trimers have an S-shaped band system at 646(−) and 659(+) nm (Csatorday *et al.*, 1984), which is replaced in AP-B by a redshifted, distorted S-shaped system of opposite sign (Fig. 2; Glazer & Bryant, 1975; Lundell & Glazer, 1983*b*; MacColl, 2004).This indicates different chromophore geometries and/or interactions in AP-B and APC trimers but similar ones in the monomers. The urea-induced dissociation kinetics were mono-exponential (Supplementary Fig. S4*c*).

3.2. Crystal structure and spherical assembly of AP-B

AP-B was crystallized in 0.5 *M* ammonium sulfate, 0.1 *M* sodium citrate tribasic dihydrate pH 5.6, 1.0 *M* lithium sulfate monohydrate (Table 1). The crystal structure was determined at 1.75 Å resolution by molecular replacement with *Phaser* using the ApcA–ApcB monomer (PDB entry 1b33; Reuter *et al.*, 1999) as a search model and was refined to a final *R* factor and free *R* factor of 0.169 and 0.193, respectively. There is one trimer $(ApcD–ApcB)_3$ in the asymmetric unit, in which the ApcD–ApcB monomers are related by noncrystallographic threefold rotational symmetry (Fig. 3). The electron-density map shows side-chain densities that are consistent with the entire sequence register of ApcD in chains *A*, *C* and *E*, with disorder in the C-terminal His-tag regions (Supplementary Fig. S5). As in the original sample, no core linker L_C was detectable. No additional protein was found in the crystal structure judging by both electron density (Supplementary Fig. S5) and electrophoresis (Supplementary Fig. S3).

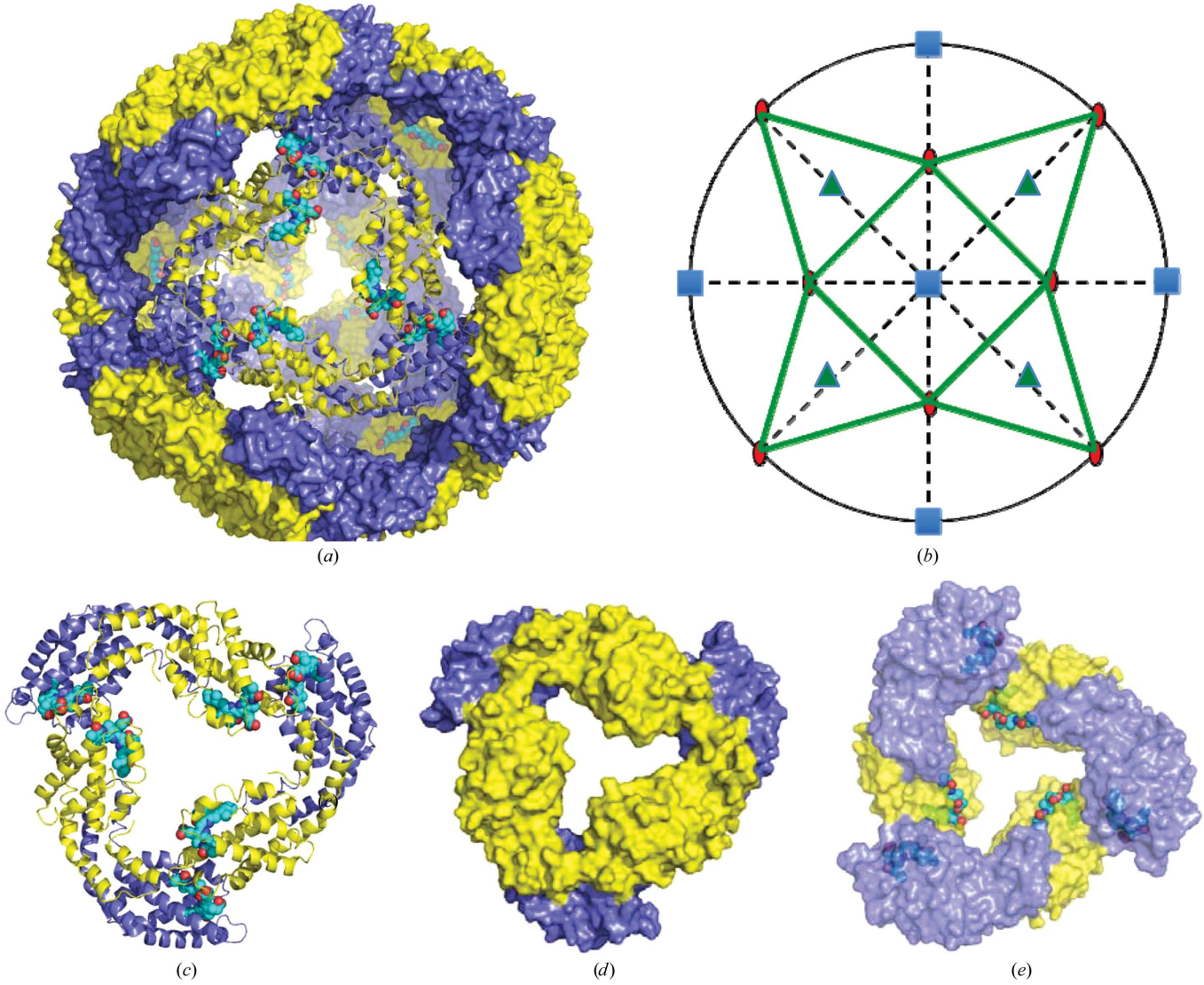

Figure 3
Crystal packing and structure of AP-B. (*a*) Eight α/β trimers form a spherical assembly in the crystal lattice. α subunits (ApcD) are coloured blue, β subunits (ApcB) yellow and the PCB chromophore cyan. One of the eight trimers is represented as a ribbon diagram. (*b*) This 48-subunit assembly adopts point group 432. The twofold (ovals), threefold (triangles) and fourfold (squares) symmetries are distributed as marked. (*c*) AP-B adopts an α/β trimeric structure typical of phycobiliproteins in PBS. (*d*) A surface representation of the AP-B structure shows interconnected β-subunits. (*e*) Viewed from the opposite side, the α-subunits are detached from one another. A semi-transparent surface of the AP-B trimer shows that the chromophores in the β-subunits are exposed to the trimer interior, while those in the α-subunits are completely buried.

In the dome-shaped ApcD–ApcB trimer, the ApcB subunits make direct contacts with one another. Three ApcD subunits join the assembly *via* extensive interactions with the ApcB subunits, but make no contacts with one another (Fig. 3). Similar triangular structures with contacting β-subunits and separated α-subunits have also been found in the more abundant phycobiliproteins, where trimers are usually stacked as hexamers and higher aggregates as in the PBS rods (Adir & Lerner, 2003; Adir *et al.*, 2002; David *et al.*, 2011; Ficner *et al.*, 1992; Liu *et al.*, 1999; Marx & Adir, 2013; Reuter *et al.*, 1999; Schirmer *et al.*, 1985, 1986; Stec *et al.*, 1999; Wang *et al.*, 2001; Brejc *et al.*, 1995).

Owing to the high symmetry in space group *I*422, eight trimers are assembled into an octahedral 'ball' consisting of a total of 48 subunits: 24 ApcB and 24 ApcD (Fig. 3). The hollow AP-B ball has an outer and inner diameter of 193 and 130 Å, respectively, and an inner space of 1.1×10^6 Å^3. Eight AP-B trimers cover the entire ball; they are related by alternating twofold, threefold and fourfold symmetries. Along the noncrystallographic threefold axis, there are triangular holes in the centres of the trimers with a maximum diameter of 52 Å. Along the fourfold symmetry axis, the holes between the adjacent trimers are square-shaped with a maximum diameter of 79 Å (Fig. 3). Extensive interactions near the twofold symmetry axes serve as joints for neighbouring AP-B trimers (Supplementary Fig. S6). As a result, the ApcB subunits form a continuous, porous inner spherical surface, while the ApcD subunits are located on the outer surface of the sphere. The structure shows a novel edge-to-edge interaction mode between adjacent trimers, with their disc planes tilted by $\sim$120°. This interface buries a surface area of about 470 Å^2 (*PISA* server; Krissinel & Henrick, 2007). The closest interactions are provided by residues 57–64 in ApcD of one trimer with residues 39–47 in ApcB of the neighbouring trimer (Fig. 3). The sequences of ApcD and ApcA differ in the contact region: amino acid 56 is mostly basic (Lys or Arg) in ApcD but is acidic in ApcA, and amino acid 65 is mostly aromatic in ApcD but is aliphatic in ApcA (Fig. 4, yellow circles). These differences may contribute to the different edge-to-edge interactions between AP-B and APC (Supplementary Fig. S6); they may be relevant to PBS assembly and to the interactions of AP-B with proteins in the membrane (Fig. 5; see §4).

For phycobiliproteins, only trimer and hexamer stacking have previously been discussed as possible PBS assembly modes (Gantt *et al.*, 2003; MacColl, 1998; Sidler, 1994; Bryant, 1991; Glazer, 1984). Spherical assemblies have been found for capsids (PDB entries 1cd3 and 1al0; Dokland *et al.*, 1997, 1999) and in icosahedral liposome phases of hydrophobic light-harvesting complexes (Liu *et al.*, 2004) and bacteriorhodopsin (Kouyama *et al.*, 1994), but in both cases the balls are larger. A more pertinent example is ferritin (PDB entry 1fha; Lawson *et al.*, 1991); it also shows a hollow octahedral assembly pattern that is relevant to its Fe-carrier function. A 24-subunit, 13 nm diameter ball with a similar octahedral assembly has been designed with the aid of general computational methods to explore self-assembling protein nanomaterials and sophisticated protein-based molecular machines (King *et al.*, 2012). Although the 48-subunit assembly of eight AP-B trimers could not be detected in solution by gel filtration (Supplementary Fig. S3), similar hollow assemblies with comparable diameters were clearly visible on a copper grid by negative-staining electron microscopy (Supplementary Fig. S7). This large spherical assembly would inspire the design of protein cages and provide a scaffold for potential nanomachinery based on phycobiliproteins.

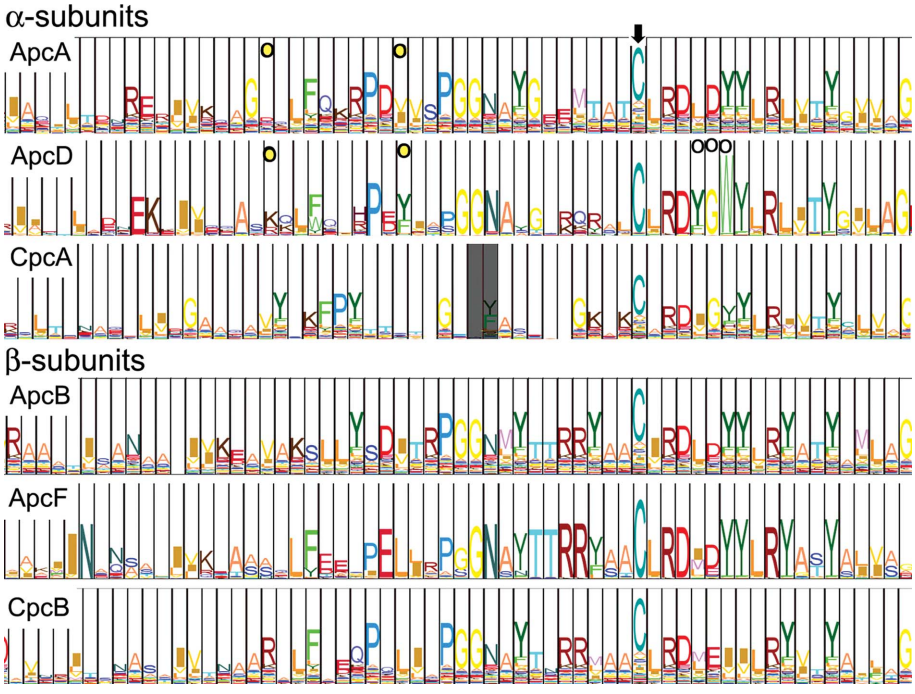

Figure 4
Sequence alignment among 60 APC and CPC subunits with pairwise HMM logos (Schuster-Böckler & Bateman, 2005). Logos were aligned with the binding cysteine (arrow) located in *Synechocystis* at position 81 in ApcA, ApcB and ApcD, at position 84 in CpcA and at position 82 in CpcB and ApcF. A signature sequence motif Y/F-G-W (residues 85-86-87 in ApcD, marked with circles) is revealed in a subfamily which is expected to show similar redshifted spectral features. The sequences of APC and CPC are taken from *Cyanidium caldarium* (NC_001840.1), *Cyanophora paradoxa* (NC_001675.1), *Galdieria sulphuraria* (KB454484.1), *Nostoc* sp. PCC 7120 (NC_003272.1), *Pyropia haitanensis* (NC_017751.1), *P. yezoensis* (KC517072.1), *Synechococcus elongatus* PCC 6301 (NC_006576.1), *Synechococcus* sp. PCC 7002 (NC_010475.1), *Synechocystis* sp. PCC 6803 (NC_000911.1) and *Thermosynechococcus elongatus* BP-1 (NC_004113.1).

3.3. PCB conformation and chromophore-binding pocket

In the crystal structure of AP-B at 1.75 Å resolution, the PCB chromophores in both subunits adopt the *ZZZ*

anti–syn–anti geometry that is typical of phycobiliproteins (Figs. 6*a* and 6*b*). In the ApcD subunits (chains *A*, *C* and *E*), PCB is covalently linked to Cys81[3] from the β-face *via* the C3^1 atom of the (original) ethylidene group of ring A. The most notable difference in PCB between the ApcD and ApcB subunits (chains *B*, *D* and *F*) is the conformation of ring D. In ApcB ring D is located at the β-face of PCB, while it is nearly coplanar with rings B and C in ApcD (Fig. 6*c*). Structural comparison among the α-subunits of CPC (Adir *et al.*, 2002), APC (Brejc *et al.*, 1995), APC-L$_C$ (Reuter *et al.*, 1999) and AP-B reveals an increasingly coplanar conformation of PCB (Fig. 7), which coincides with the absorption maximum being redshifted in the same order. Since the conjugation system of PCB extends to ring D, the unique conformation of PCB in ApcD is likely to contribute to the most redshifted absorption of AP-B (λ_{max} = 669 nm; Fig. 2).

The carbonyl group and the pyrrole N atom of ring D form direct and water-mediated hydrogen bonds to the main-chain atoms of the conserved Tyr62, Thr66, Met72 and Thr74 in ApcB of the adjacent monomer (Fig. 6*e*). Interestingly, the hydrogen bond between the carbonyl O atom of ring D in ApcD and the main-chain N atom of Thr74 of ApcB (with a distance of 2.89 Å; Fig. 6*e*) leads to backbone distortion near Thr74 such that Thr74 is the only residue that is located in the disallowed region of the Ramachandran plot despite the well resolved electron densities (Supplementary Fig. S5). These close intersubunit interactions further stabilize the coplanar conformation of ring D with rings B and C of the PCB in ApcD (Supplementary Fig. S8). They are also found in the APC trimer (PDB entry 1b33). This chromophore conformation that is stabilized by the highly conserved hydrogen bonds between the α-subunits and β-subunits from adjacent monomers probably accounts for the additional redshift induced by the trimer formation (Supplementary Fig. S4); it distinguishes allophycocyanins from phycocyanins. Two conserved residues corresponding to Tyr116 and Asp84 of ApcD (also found in ApcA and ApcB) form a short hydrogen bond. Although they are located on opposite faces of PCB (Fig. 8; Supplementary Fig. S8), they would contribute to stabilizing the PCB conformation. In ApcD from *Nostoc*, the mutation Y116S in ApcD abolishes the redshifted phenotype (Supplementary Table S3; Wang *et al.*, 2010).

In the APC trimer, the chromophore-binding pocket in the α-subunit (ApcA) is in general more enclosed than that of the β-subunit (ApcB) (Brejc *et al.*, 1995). Such a hydrophobic first shell of the chromophore, surrounded by a highly charged second shell, has been identified by McGregor *et al.* (2008) as a characteristic of APC, which is supported by the AP-B structure (see §4). The chromophore-binding pocket in ApcD appears to be even tighter than that in ApcA (Fig. 3*d*). Ring D in ApcD is sandwiched between the bulky side chains of Met115 and Trp87 *via* van der Waals interactions (Fig. 8). Of the 17 ApcD residues that are in direct contact (<3.7 Å) with PCB, six residues (Tyr65, Asn71, Gln80, Tyr85, Trp87 and Met126) differ from those in ApcA; in all six varied residues in ApcD carries bulkier side chains than in ApcA. We speculate that these bulkier side chains surrounding the chromophore lead to compaction of the pocket (Fig. 8), which enhances the coplanarity of rings B, C and D (Figs. 6 and 7) and eventually leads to the redshifted absorption of ApcD (Fig. 2, Supplementary Tables S3 and S4). To test our hypothesis, five ApcD single mutants (W87Y, Q80T, Y65V, Y85L and M126V) were produced around the chromophore-binding pocket which convert these residues to the respective residues of ApcA (Supplementary Table S1). The spectra of all of these mutants were significantly affected; most of them, particularly those from *Nostoc* sp. PCC 7120 (Supplementary Table S3), are blueshifted compared with the wild-type subunit and showed broadened, structured bands indicative of heterogeneity (Fig. 8, Supplementary Fig. S9, Supplementary Table S3). These data support a contribution of tighter and snugger fitting with the concomitant coplanar conformation of PCB in its pocket to the redshift in ApcD. However, the shifts are not additive; some single mutants even exhibit redshifts. Rather,

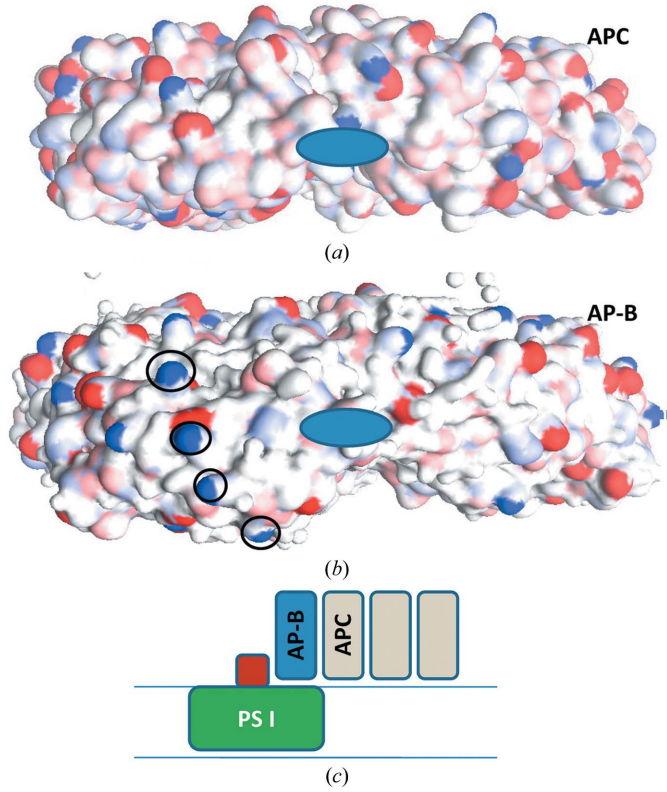

Figure 5
Possible assembly of AP-B with PSI. Trimers of (*a*) APC (PDB entry 1b33) and (*b*) AP-B (this work) seen side-on with the α-subunit (ApcA and ApcD, respectively) on the left and the β-subunit (ApcB) on the right. The blue ellipse indicates the position of the chromophore on the α-subunit near the surface. The rim of positively charged amino acids on ApcD is marked by circles. (*c*) Schematic putative arrangement of PSI (green) with the iron–sulfur protein F$_{A,B}$ (red) protruding from the membrane into the cytoplasm and a rod of the phycobilisome core consisting of trimers of AP-B (blue) at the end; other APCs are shown in grey. Plots were generated with *Discovery Studio* v.3.5 (Accelrys).

[3] Here and in the figures the actual amino-acid numbering has been used: Cys81 of ApcD from *Synechocystis* corresponds to Cys84 in the consensus numbering of phycobiliproteins.

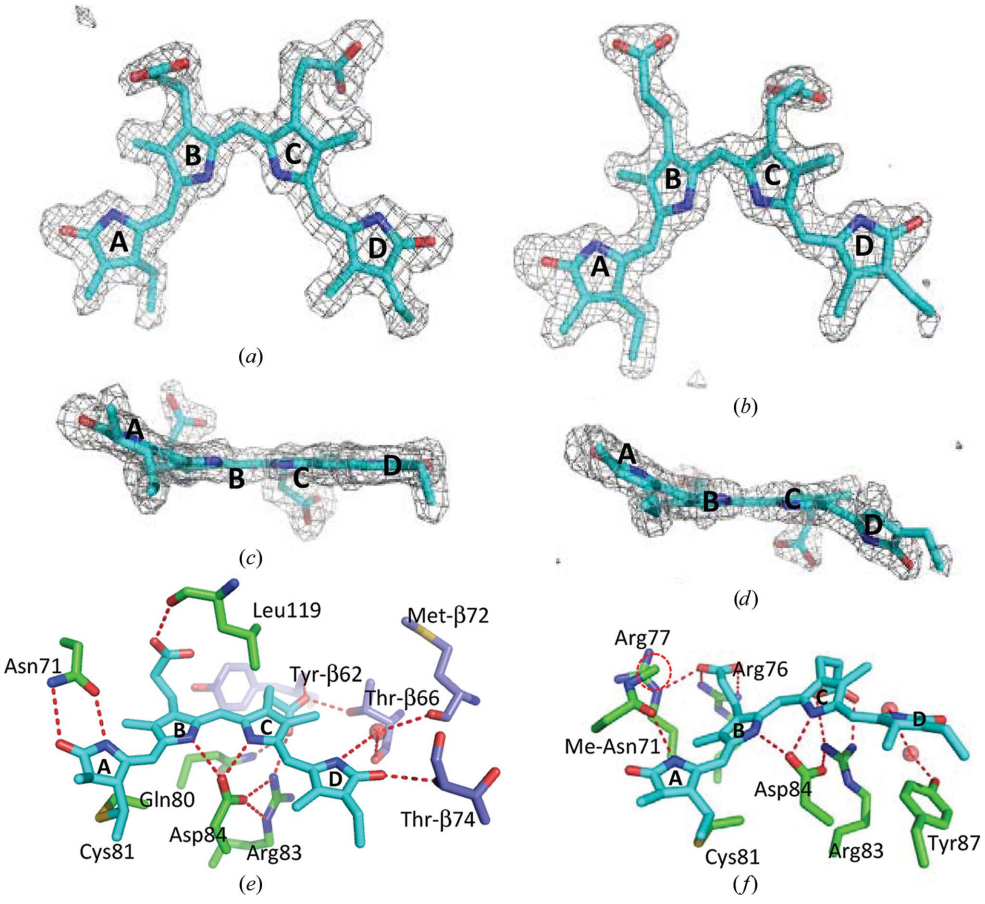

Figure 6
Conformations and protein environments of the chromophores in the AP-B structure. Simulated-annealing OMIT maps for PCB in the α-subunit (ApcD) (*a*) and the β-subunit (ApcB) (*b*) show that both chromophores adopt *ZZZ anti–syn–anti* conformations. Side views of (*a*) and (*b*) show different dispositions of ring D. In the α-subunit rings B, C and D are nearly coplanar (*c*), while in the β-subunit ring D is located on the β-face of PCB (*d*). (*e*) PCB in the α-subunit is involved in extensive hydrogen-bond interactions (red dashed lines) with residues of both the same subunit (green) and the neighbouring subunit (purple). (*f*) PCB is stabilized by hydrogen bonds in the β-subunit, where rings C and D are exposed to the solvent. Asn71 in the β-subunit is methylated (the methyl group is marked by a red dashed circle) and interacts with the pyrrole N atom of ring A. Both PCB are covalently linked to the protein moiety *via* a thioether bond between Cys81 and the $C3^1$ atom of ring A.

the variations surrounding the chromophore collectively ensure that ring D is coplanar with rings B and C in ApcD. The redshift in absorption maxima shows a remarkable correlation with the extent of coplanarity in the PCB chromophore (Fig. 7*b*, Supplementary Table S4). In contrast to the trimer-induced redshift discussed in the previous section, these interactions are entirely intramolecular; they rationalize the site-specific redshift in isolated ApcD (Wang *et al.*, 2010; Zhao, Su *et al.*, 2007; Lundell & Glazer, 1981).

Trp87 evidently enhances the snug fitting of ring D into its pocket compared with Tyr87 in ApcA. A sequence alignment among 60 APC subunits, together with our structural analyses, reveals a signature sequence motif Y/F-G-W (residues 85-86-87) in the ApcD subfamily. In contrast, ApcA and ApcB have Tyr at this position (Fig. 4). Although we have not yet obtained a Trp87 mutant of ApcD from *Synechocystis*, ApcD(W87Y) assembled in *E. coli* displays distinctly blue-shifted absorption and fluorescence compared with wild-type ApcD (Supplementary Table S3; Wang *et al.*, 2010); it absorbs like chromophorylated ApcA or ApcB (Fig. 8, Supplementary Table S3). An even more pronounced blueshift has been observed for the ApcD(W87E) mutant of *Nostoc* (Supplementary Table S3).

Another difference between ApcD and ApcA is the conformation of Asn71, which forms a strong hydrogen bond to the pyrrolic N atom of ring A of PCB (Fig. 6*e*). Asn71 is methylated in ApcB but not in ApcA and ApcD (Figs. 6*e* and 6*f*). The conformation of Asn71 in ApcD is significantly different from that in ApcA (Reuter *et al.*, 1999; Fig. 8, Supplementary Fig. S8), resulting in very different dihedral angles between rings A and B in the PCB chromophore (Supplementary Table S4). In ApcD, the unmethylated Asn71 forms double hydrogen bonds to ring A (Fig. 6*e*) which are possibly facilitated by the nearby Tyr65. Mutation of this Tyr to Val induced a blueshift in ApcD (Supplementary Fig. S9, Supplementary Table S3), suggesting that the conformation of ring A also contributes to the site-specific redshift of PCB in ApcD.

4. Discussion

Among the morphologically distinct PBSs (Reuter *et al.*, 1990; Ducret *et al.*, 1998), the hemidiscoidal type is the best char-

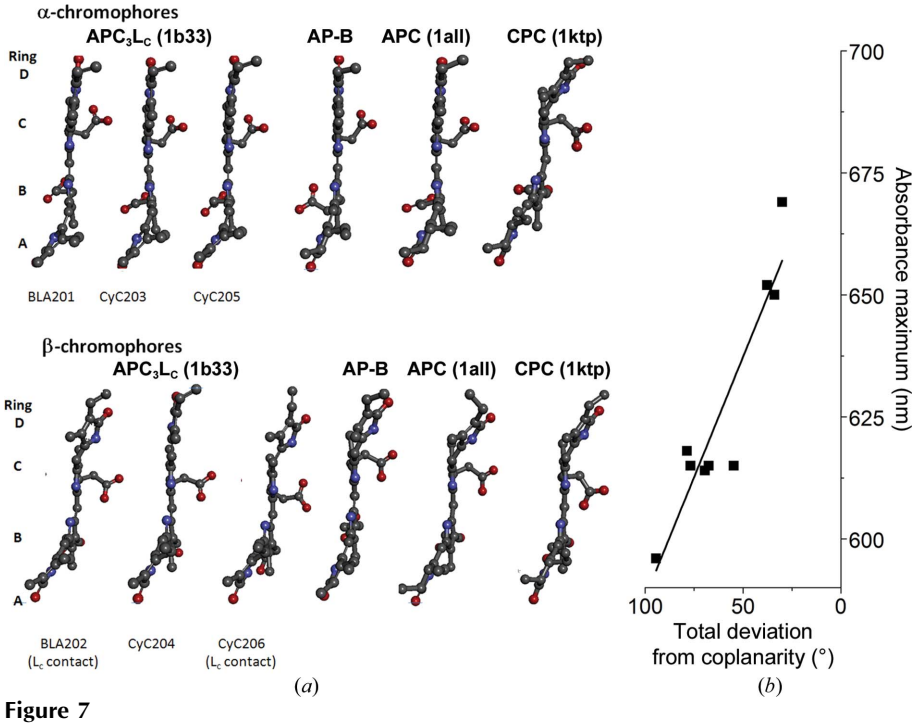

Figure 7
Comparison of the PCB conformations in the α-subunits (top) and β-subunits (bottom) of CPC_3 (PDB entry 1ktp; Adir *et al.*, 2002), APC_3 (PDB entry 1all; Brejc *et al.*, 1995), APC_3L_C (PDB entry 1b33; Reuter *et al.*, 1999) and AP-B (this work). (*a*) The tetrapyrrole system is seen sideways in the plane of rings B and C; with ring A at the bottom. PDB codes are given in parentheses. The chromophores of the individual monomers of APC_3L_C are labelled as in PDB entry 1b33 (Reuter *et al.*, 1999). Plots were generated with *Discovery Studio* v.3.5 (Accelrys). (*b*) Linear fit of the position of the long-wavelength absorption maximum with the planarity of the PCB chromophore, as defined by the sum of the twists between adjacent rings (see Supplementary Table S4 for details).

acterized and widespread in cyanobacteria. Four different complexes have been isolated from its core by controlled dissociation. In addition to the APC trimer, these are heterogeneous trimers of allophycocyanins that also contain linkers (Bryant, 1991; Sidler, 1994; Ducret *et al.*, 1998). Among them, $(ApcA_2ApcD_1ApcB_3)L_C$ and $(ApcA_2ApcB_2ApcF_1)$-L_{CM} serve as energy-transfer units to the photosystems, where the low-energy chromophores in ApcD and L_{CM} are identified as terminal emitters[4].

Instead, we used His-tagged ApcD to isolate the linker-free complex $(ApcD–ApcB)_3$ by Ni^{2+}-affinity chromatography and gel filtration. Depending on the ionic strength of the KPB used to break the cells and for affinity chromatography, AP-B containing the His-tagged ApcD could be isolated directly at low ionic strength or *via* phycobilisomes (high ionic strength), from which it was then purified by subfractionation in PBS (Lundell & Glazer, 1983*a*; Reuter *et al.*, 1990, 1999; Ducret *et al.*, 1998; Brejc *et al.*, 1995; Glazer & Bryant, 1975). In some cases, complexes containing two α-subunits, ApcA and ApcD, were obtained. Interestingly, this heterogeneity was lost in the crystals, perhaps owing to complete subunit shuffling (Lundell & Glazer, 1983*a*). This allowed the high-resolution structure of a terminal emitter to be determined for the first time. Obviously, $(ApcD–ApcB)_3$ was more liable to crystallization, possibly owing to the affinity enrichment of ApcD and/or high stability of the complexes in the crystal lattice of high symmetry (Table 1).

There is only little interaction among the α-subunits that would significantly affect the optical spectra. In agreement, the redmost absorption of the ApcD–ApcB trimer matches well that of natural AP-B with or without a linker; natural AP-B contains two ApcA and only one ApcD in the trimer (Glazer & Bryant, 1975; Lundell & Glazer, 1981, 1983*a*; Reuter *et al.*, 1990). In the following discussion, we assume that the situation of the ApcD chromophores observed in the $(ApcD–ApcB)_3$ trimer is comparable to that of the single ApcD chromophore in AP-B. The spectra of bilins are very sensitive to their conformations (Mroginski *et al.*, 2009; Petrier *et al.*, 1981; Inomata, 2008); steric interaction with bulky residues is therefore a means of spectral tuning. The structure rationalizes that the large redshift of AP-B is owing to the ApcD chromophore, which is held in an essentially coplanar conformation of the conjugation system. A comparison with PCB in various binding sites gives a good correlation of the redshift with a twist of ring D out of the plane of rings B and C (Fig. 7). When this correlation is extrapolated to perfect coplanarity of all four rings (Fig. 7*b*), the PCB chromophore would absorb maximally at 686 nm. An additional contribution may result from π–π interactions with Trp87 of ApcD that strongly affects the spectrum (Supplementary Table S3).

Both subunits contribute to steric conferring of the planar conformation on the ApcD chromophore. In the absence of the X-ray structures of isolated subunits, we used the trimer to assess the intramolecular interactions. One face of the PCB chromophore in α-subunits of phycobiliproteins interacts with residues of this subunit. Sequence alignment among different PCB-bearing subunits shows that the residues at this site are prevalently bulkier in ApcD than in ApcA, ApcB, CpcA and CpcB (Figs. 4 and 8). This correlates with a redshifted absorption of the ApcD chromophore (λ_{max} = 625–650 nm, species-dependent; Supplementary Table S3; see also Lundell & Glazer, 1981) that sets it apart from all other PCBs in phycobiliprotein α-subunits (λ_{max} = 610–620 nm).

In trimers, the other face of the α-chromophore interacts with residues of the β-subunit of the neighbouring monomer. Here, allophycocyanins, including AP-B, differ substantially from phycocyanins, in particular in the hydrogen-bonding

[4] The rod–core linker CpcG2 has been implicated as an additional emitter in *Synechococcus* PCC7002 (Deng *et al.*, 2012); this linker is absent in many cyanobacteria, including *Synechocystis*.

network to ring D (Supplementary Fig. S8). The tighter hydrogen bonds correlate with an aggregation-induced redshift of ∼30 nm in allophycocyanins compared with only ∼15 nm in phycocyanins.

Two additional or alternative contributions to the redshift of trimeric APCs compared with CPCs have been discussed. The mechanism of polar-enhanced hydrophobicity (McGregor *et al.*, 2008) is based on two shells surrounding the α-84 chromophore (consensus numbering). An inner hydrophobic shell enhances the redshifting effect of the polar outer shell on the π–π^* transitions. This model gained support from the larger number of polar residues in the outer shell of APC compared with CPC. The number of polar residues in AP-B is also larger than in CPC, indicating a contribution of this effect. The number is, however, lower than in APC $(\text{ApcA–ApcB})_3$, in spite of the even larger redshift.

A third origin for the aggregation-induced redshift is excitonic interaction, as first proposed from the intense S-shaped CD signals that develop on the trimerization of APC (Csatorday *et al.*, 1984). However, such strong signals can also arise from conformational changes of the inherently asymmetric bilin chromophores in a protein environment (see, for example, Falk, 1989; Krois & Lehner, 1987). In the crystal structure of APC from *Spirulina platensis* (Brejc *et al.*, 1995), the relevant chromophore geometries and their centre-to-centre distance of 21 Å are at the limit of significant excitonic coupling. The distances and orientations are moreover very similar to those of CPC from various cyanobacteria, where the redshifts are much smaller (David *et al.*, 2011; Jiang *et al.*, 2001; Schirmer *et al.*, 1987). For CPC trimers from *Synechococcus* PCC7002, energy-transfer kinetics in trimers were fitted well by a Förster hopping model with localized excitations (Debreczeny *et al.*, 1995*a*,*b*). Femtosecond depolarization studies of APC trimers also suggested only weak coupling of the redshifted chromophores (Sharkov *et al.*, 1992, 1994), while subsequent work supported strong coupling (Womick *et al.*, 2010; Womick & Moran, 2009; Edington *et al.*, 1996; Homoelle *et al.*, 1998). These conflicting data reflect the borderline situation between strong and weak coupling given by the structures of APC trimers (Holzwarth *et al.*, 1990). The distances between the chromophores from two adjacent dimers are also similar in AP-B trimers. They even seem slightly larger than in APC-L_C (Supplementary Fig. S10), in agreement with an overall slight flattening of the trimer. Assuming otherwise similar factors, this would further reduce excitonic coupling between α- and β-chromophores.

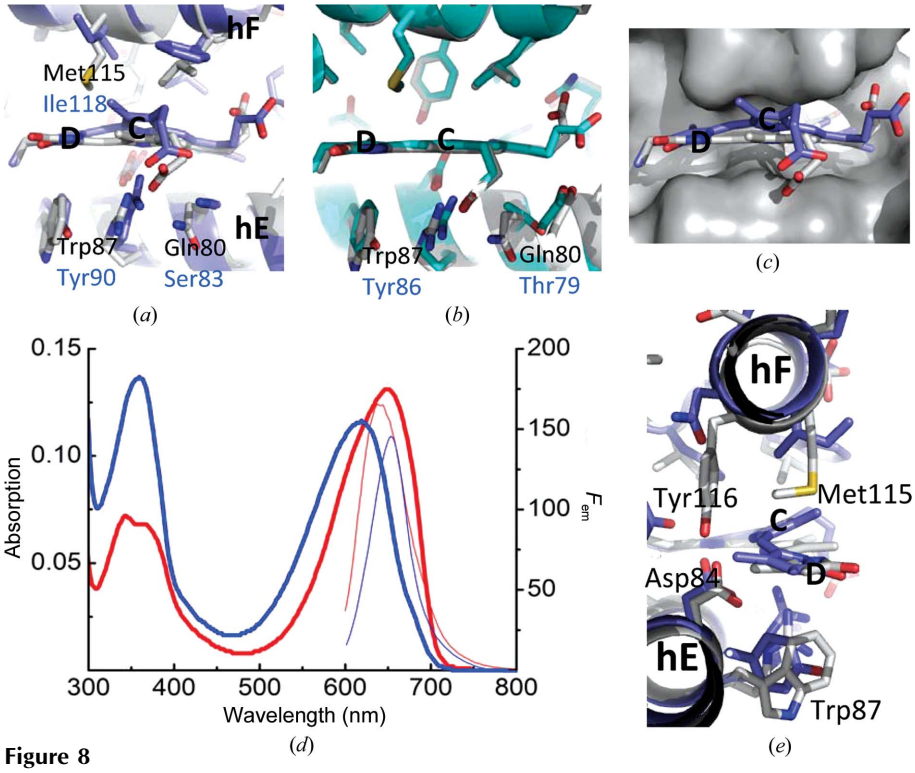

Figure 8
Structural comparisons in the chromophore-binding pocket among α-subunits of CPC (PDB entry 3l0f; blue), APC (PDB entry 1b33; cyan) and AP-B (grey). (*a*) Superposition of CPC and APC shows different PCB conformations that are buried in cavities of distinct shape. (*b*) AP-B and APC align well at the α-face of the chromophore, while AP-B exhibits bulkier side chains on the β-face of PCB, thus rendering a tighter chromophore pocket. (*c*) The snug chromophore pocket in AP-B is not compatible with the PCB conformation of CPC (blue). (*d*) Absorption (thick lines) and fluorescence (thin lines) spectra of chromophorylated ApcD(Q80T) (red) and ApcD(W87Y) (blue); further data are shown in Supplementary Fig S9 and Supplementary Table S3. (*e*) A side view of (*a*) shows that rings C and D are sandwiched between two helices, hE and hF, from which bulky side chains (Trp87, Tyr116 and Met115) accommodate a flat chromophore conformation. Residues are labelled as in AP-B.

AP-B is one of the terminal emitters; it has been implicated in energy transfer to and protection of photosystem I (Dong *et al.*, 2009; Liu *et al.*, 2013). The outward-facing surface of ApcD near the chromophore differs substantially from that of ApcA; in particular, there is a rim of roughly evenly spaced positively charged amino acids near the chromophore that could promote the differential interaction (Fig. 5). These are the same amino acids that are involved in the unusual crystal packing (see above). If the receptor protein contains chlorophyll near the site of interaction, this would bring the long-wavelength emitting ApcD chromophore to a favourable distance for efficient Förster transfer. Quenching centres such as carotenoids would need much shorter distances for Dexter transfer. The PSI core complex would qualify as such an acceptor protein, and docking studies using *Hex* (Ritchie & Kemp, 2000) showed acceptable solutions with the trimer axis oriented parallel to the membrane and the ring-shaped trimer sitting side-on such that the periphery touches the cytoplasmic surface of PsbA or PsbB. This would allow an arrangement of the core rods as shown in Fig. 5(*c*), which compares well with the model proposed by Liu *et al.* (2013).

A most interesting feature of the AP-B crystal structure is the molecular packing of 48 subunits in the crystal lattice (Fig. 3), in which APC subunits form a porous hollow ball *via* edge-to-edge interactions between ApcD and ApcB subunits (Supplementary Fig. S6). These edge-to-edge interactions differ from those of other biliproteins (Adir & Lerner, 2003; David *et al.*, 2011; Marx & Adir, 2013) and may relate to interactions with PBS rods or with components of the photosynthetic membrane. The unique 48-subunit ball-like packing of AP-B would furthermore inspire molecular designs for protein cages (King *et al.*, 2012), optoelectric biomaterials and biomolecular devices based on phycobiliproteins. The size of the packing ball, the volume of internal space and the openings on the surface are very promising for nano-machinery. One can attach certain functional units to these phycobiliprotein subunits and position other functional units at the centre. For example, with photophysical and/or photochemical units absorbing at longer wavelengths placed at the centre, the chromophores of APC would function as antenna with an enhanced photochemical cross-section.

5. Related literature

The following references are cited in the Supporting Information for this article: Contreras-Martel *et al.* (2007), Duerring *et al.* (1991), Zhao *et al.* (2006) and Zhao, Zhang *et al.* (2007).

We thank Kun Tang and Ming Zhou (Wuhan, China) for experimental assistance. This work was supported by the National Natural Science Foundation of China (grants 31110103912 and 31270893 to K-HZ) and the State Key Laboratory of Agricultural Microbiology. XY acknowledges support from the Department of Biochemistry and Molecular Biology and the Moffat laboratory at the University of Chicago. P-PP acknowledges support (2013SC03) from the Fundamental Research Funds for the Central Universities. We thank the LS-CAT staff at Advanced Photon Source, Argonne National Laboratory for beamline support. Use of the Advanced Photon Source was supported by the US Department of Energy, Office of Science, Office of Basic Energy Sciences, under Contract No. DE-AC02-06CH11357.

References

Adams, P. D. *et al.* (2010). *Acta Cryst.* D**66**, 213–221.
Adir, N. & Lerner, N. (2003). *J. Biol. Chem.* **278**, 25926–25932.
Adir, N., Vainer, R. & Lerner, N. (2002). *Biochim. Biophys. Acta*, **1556**, 168–174.
Berkelman, T. R. & Lagarias, J. C. (1986). *Anal. Biochem.* **156**, 194–201.
Bradford, M. M. (1976). *Anal. Biochem.* **72**, 248–254.
Brejc, K., Ficner, R., Huber, R. & Steinbacher, S. (1995). *J. Mol. Biol.* **249**, 424–440.
Bryant, D. A. (1991). *Cell Culture and Somatic Cell Genetics of Plants*, Vol. 7B, *The Photosynthetic Apparatus: Molecular Biology and Operation*, edited by L. Bogorad & I. K. Vasil, pp. 257–300. New York: Academic Press.
Cai, Y. A., Murphy, J. T., Wedemayer, G. J. & Glazer, A. N. (2001). *Anal. Biochem.* **290**, 186–204.
Contreras-Martel, C., Matamala, A., Bruna, C., Poo-Caamaño, G., Almonacid, D., Figueroa, M., Martínez-Oyanedel, J. & Bunster, M. (2007). *Biophys. Chem.* **125**, 388–396.
Csatorday, K., MacColl, R., Csizmadia, V., Grabowski, J. & Bagyinka, C. (1984). *Biochemistry*, **23**, 6466–6470.
David, L., Marx, A. & Adir, N. (2011). *J. Mol. Biol.* **405**, 201–213.
Debreczeny, M. P., Sauer, K., Zhou, J. & Bryant, D. A. (1995*a*). *J. Phys. Chem.* **99**, 8412–8419.
Debreczeny, M. P., Sauer, K., Zhou, J. & Bryant, D. A. (1995*b*). *J. Phys. Chem.* **99**, 8420–8431.
Deng, G., Liu, F., Liu, X. & Zhao, J. (2012). *FEBS Lett.* **586**, 2342–2345.
Dokland, T., Bernal, R. A., Burch, A., Pletnev, S., Fane, B. A. & Rossmann, M. G. (1999). *J. Mol. Biol.* **288**, 595–608.
Dokland, T., McKenna, R., Ilag, L. L., Bowman, B. R., Incardona, N. L., Fane, B. A. & Rossmann, M. G. (1997). *Nature (London)*, **389**, 308–313.
Dong, C., Tang, A., Zhao, J., Mullineaux, C. W., Shen, G. & Bryant, D. A. (2009). *Biochim. Biophys. Acta*, **1787**, 1122–1128.
Ducret, A., Müller, S. A., Goldie, K. N., Hefti, A., Sidler, W. A., Zuber, H. & Engel, A. (1998). *J. Mol. Biol.* **278**, 369–388.
Duerring, M., Schmidt, G. B. & Huber, R. (1991). *J. Mol. Biol.* **217**, 577–592.
Edington, M. D., Riter, R. E. & Beck, W. F. (1996). *J. Phys. Chem.* **100**, 14206–14217.
Falk, H. (1989). *The Chemistry of Linear Oligopyrroles and Bile Pigments.* Vienna: Springer.
Ficner, R., Lobeck, K., Schmidt, G. & Huber, R. (1992). *J. Mol. Biol.* **228**, 935–950.
Gantt, B., Grabowski, B. & Cunningham, F. X. (2003). *Light-Harvesting Antennas in Photosynthesis*, edited by B. Green & W. Parson, pp. 307–322. Dordrecht: Kluwer.
Gingrich, J. C., Lundell, D. J. & Glazer, A. N. (1983). *J. Cell. Biochem.* **22**, 1–14.
Glazer, A. N. (1984). *Biochim. Biophys. Acta*, **768**, 29–51.
Glazer, A. N. & Bryant, D. A. (1975). *Arch. Microbiol.* **104**, 15–22.
Glazer, A. N. & Fang, S. (1973). *J. Biol. Chem.* **248**, 659–662.
Golden, S. S., Brusslan, J. & Haselkorn, R. (1987). *Methods Enzymol.* **153**, 215–231.
Holzwarth, A. R., Bittersmann, E., Reuter, W. & Wehrmeyer, W. (1990). *Biophys. J.* **57**, 133–145.
Homoelle, B. J., Edington, M. D., Diffey, W. M. & Beck, W. F. (1998). *J. Phys. Chem.* **102**, 3044–3052.
Inomata, K. (2008). *Bull. Chem. Soc. Jpn*, **81**, 25–59.
Jiang, T., Zhang, J.-P., Chang, W.-R. & Liang, D.-C. (2001). *Biophys. J.* **81**, 1171–1179.
King, N. P., Sheffler, W., Sawaya, M. R., Vollmar, B. S., Sumida, J. P., André, I., Gonen, T., Yeates, T. O. & Baker, D. (2012). *Science*, **336**, 1171–1174.
Kouyama, T., Yamamoto, M., Kamiya, N., Iwasaki, H., Ueki, T. & Sakurai, I. (1994). *J. Mol. Biol.* **236**, 990–994.
Krissinel, E. & Henrick, K. (2007). *J. Mol. Biol.* **372**, 774–797.
Krois, D. & Lehner, H. (1987). *J. Chem. Soc. Perkin Trans. 2*, pp. 219–225.
Laemmli, U. K. (1970). *Nature (London)*, **227**, 680–685.
Lawson, D. M., Artymiuk, P. J., Yewdall, S. J., Smith, J. M., Livingstone, J. C., Treffry, A., Luzzago, A., Levi, S., Arosio, P., Cesareni, G., Thomas, C. D., Shaw, W. V. & Harrison, P. M. (1991). *Nature (London)*, **349**, 541–544.
Liu, H., Zhang, H., Niedzwiedzki, D. M., Prado, M., He, G., Gross, M. L. & Blankenship, R. E. (2013). *Science*, **342**, 1104–1107.
Liu, J.-Y., Jiang, T., Zhang, J.-P. & Liang, D.-C. (1999). *J. Biol. Chem.* **274**, 16945–16952.
Liu, Z., Yan, H., Wang, K., Kuang, T., Zhang, J., Gui, L., An, X. & Chang, W. (2004). *Nature (London)*, **428**, 287–292.
Lundell, D. J. & Glazer, A. N. (1981). *J. Biol. Chem.* **256**, 12600–12606.

Lundell, D. J. & Glazer, A. N. (1983*a*). *J. Biol. Chem.* **258**, 902–908.
Lundell, D. J. & Glazer, A. N. (1983*b*). *J. Biol. Chem.* **258**, 8708–8713.
MacColl, R. (1998). *J. Struct. Biol.* **124**, 311–334.
MacColl, R. (2004). *Biochim. Biophys. Acta*, **1657**, 73–81.
Marx, A. & Adir, N. (2013). *Biochim. Biophys. Acta*, **1827**, 311–318.
McGregor, A., Klartag, M., David, L. & Adir, N. (2008). *J. Mol. Biol.* **384**, 406–421.
Mroginski, M. A., von Stetten, D., Escobar, F. V., Strauss, H. M., Kaminski, S., Scheerer, P., Günther, M., Murgida, D. H., Schmieder, P., Bongards, C., Gärtner, W., Mailliet, J., Hughes, J., Essen, L. O. & Hildebrandt, P. (2009). *Biophys. J.* **96**, 4153–4163.
Otwinowski, Z. & Minor, W. (1997). *Methods Enzymol.* **276**, 307–326.
Petrier, C., Jardon, P., Dupuy, C. & Gautron, R. (1981). *J. Chim. Phys.* **78**, 519–525.
Redecker, D., Wehrmeyer, W. & Reuter, W. (1993). *Eur. J. Cell Biol.* **62**, 442–450.
Reuter, W., Nickel, C. & Wehrmeyer, W. (1990). *FEBS Lett.* **273**, 155–158.
Reuter, W., Wiegand, G., Huber, R. & Than, M. E. (1999). *Proc. Natl Acad. Sci. USA*, **96**, 1363–1368.
Ritchie, D. W. & Kemp, G. J. L. (2000). *Proteins*, **39**, 178–194.
Sambrook, J., Fritsch, E. & Maniatis, T. (1989). *Molecular Cloning: A Laboratory Manual*, 2nd ed. New York: Cold Spring Harbor Laboratory Press.
Schirmer, T., Bode, W. & Huber, R. (1987). *J. Mol. Biol.* **196**, 677–695.
Schirmer, T., Bode, W., Huber, R., Sidler, W. & Zuber, H. (1985). *J. Mol. Biol.* **184**, 257–277.
Schirmer, T., Huber, R., Schneider, M., Bode, W., Miller, M. & Hackert, M. L. (1986). *J. Mol. Biol.* **188**, 651–676.
Schuster-Böckler, B. & Bateman, A. (2005). *Bioinformatics*, **21**, 2912–2913.
Sharkov, A. V., Kryukov, I. V., Khoroshilov, E. V., Kryukov, P. G., Fischer, R., Scheer, H. & Gillbro, T. (1992). *Chem. Phys. Lett.* **191**, 633–638.
Sharkov, A. V., Kryukov, I. V., Khoroshilov, E. V., Kryukov, P. G., Fischer, R., Scheer, H. & Gillbro, T. (1994). *Biochim. Biophys. Acta*, **1188**, 349–356.
Sidler, W. A. (1994). *The Molecular Biology of Cyanobacteria*, edited by D. A. Bryant, pp. 139–216. Dordrecht: Kluwer.
Sokolenko, A., Pojidaeva, E., Zinchenko, V., Panichkin, V., Glaser, V. M., Herrmann, R. G. & Shestakov, S. V. (2002). *Curr. Genet.* **41**, 291–310.
Stec, B., Troxler, R. F. & Teeter, M. M. (1999). *Biophys. J.* **76**, 2912–2921.
Wang, X.-Q., Li, L.-N., Chang, W.-R., Zhang, J.-P., Gui, L.-L., Guo, B.-J. & Liang, D.-C. (2001). *Acta Cryst.* D**57**, 784–792.
Wang, X., Zhang, Q., Yang, B., Zhao, K.-H. & Zhou, M. (2010). *Prog. Biochem. Biophys.* **37**, 549–557.
Womick, J. M., Miller, S. A. & Moran, A. M. (2010). *J. Chem. Phys.* **133**, 024507.
Womick, J. M. & Moran, A. M. (2009). *J. Phys. Chem. B*, **113**, 15747–15759.
Zhao, K.-H., Su, P., Li, J., Tu, J.-M., Zhou, M., Bubenzer, C. & Scheer, H. (2006). *J. Biol. Chem.* **281**, 8573–8581.
Zhao, K.-H., Su, P., Tu, J. M., Wang, X., Liu, H., Plöscher, M., Eichacker, L., Yang, B., Zhou, M. & Scheer, H. (2007). *Proc. Natl Acad. Sci. USA*, **104**, 14300–14305.
Zhao, K.-H., Zhang, J., Tu, J.-M., Böhm, S., Plöscher, M., Eichacker, L., Bubenzer, C., Scheer, H., Wang, X. & Zhou, M. (2007). *J. Biol. Chem.* **282**, 34093–34103.